Published by :
http://www.ijert.org

International Journal of Engineering Research & Technology (IJERT)
ISSN: 2278-0181
Vol. 5 Issue 01, January-2016

Experimental and Numerical Study of the Split Tensile Test on a Silty Soil : Discrete Element Analysis

Abdelkader Ammeri, Mondher Neifar, Khaled Ibrahim, Mounir Bouassida*
Umm Al-Qura University
College of Engineering at Al-Qunfudah
Al-Qunfudah, Kingdom of Saudi Arabia
* Université de Tunis El Manar, École Nationale d'Ingénieurs de Tunis,
LR14ES03, Ingénierie Géotechnique. BP 37 Le Belvédère 1002 Tunis, Tunisia.

***Abstract*—An analysis of the split tensile test is conducted on a silty soil. This paper is concerned with the numerical and experimental analysis for the basic assumptions: elasticity, brittleness and in-center crack initiation. Numerical results show that the Hertz stress field is valid until failure, which guarantee the elasticity and the brittleness. However the in-center crack initiation was guaranteed only by a flattened disc. A valid loading angle corresponding to the flat end width has to be between 12° and 15°. However, numerical results show that the Hertz solution is no longer valid for the flattened disc. Therefore the calculated value of the tensile strength derived from the test and based on the Griffith failure criterion does not correspond to the uniaxial tensile strength.**

Keywords—split tensile test; uniaxial tensile strength; validity; silty soil; distinct element method

I. INTRODUCTION

The tensile strength of cohesive soils, which remains difficult to obtain by direct tensile tests, despite attempts[1][2], is the subject of several studies [3][4][5]. Indirect tensile tests are the alternative to the direct tensile test and have been widely used [6][7][8]. Several indirect tensile tests were used. But the most commonly used is the split tensile test also known as the Brazilian test thanks to its simplicity of realization. This test is already standardized for brittle materials as rocks [9] and concrete [10], it has been extended by several authors to cohesive soils with low plasticity [7][12].

The validity of the formulas used in the interpretation of the split tensile test is based on two assumptions, which are characteristics of the material : elasticity and brittle behavior. Note that the assumption of elasticity is required to use the stress field solution, developed by Hertz, while the assumption of brittleness allows extension of the stress solution to the point of failure. Furthermore, the assumption of the brittle behavior is necessary for the material to obey Griffith failure criterion.

Hertz solution and Griffith failure criterion are the basis of the theoretical interpretation of the Brazilian test as an indirect tensile test, leading to the determination of the uniaxial tensile strength.

The Hertz solution leads to the following stress field:

$$\sigma_x = \frac{-2F}{\pi h}\left(\frac{x^2(R-y)}{\beta_1^4} + \frac{x^2(R+y)}{\beta_2^4} - \frac{1}{2R}\right) \quad (1)$$

$$\sigma_y = \frac{-2F}{\pi h}\left(\frac{(R-y)^3}{\beta_1^4} + \frac{(R+y)^3}{\beta_2^4} - \frac{1}{2R}\right) \quad (2)$$

$$\sigma_{xy} = \frac{2F}{\pi h}\left(\frac{x(R-y)^2}{\beta_1^4} + \frac{x(R+y)^2}{\beta_2^4}\right) \quad (3)$$

where

$$\beta_1^2 = (R-y)^2 + x^2 \quad (4)$$

$$\beta_2^2 = (R+y)^2 + x^2 \quad (5)$$

The Griffith failure criterion is defined by:

$$\sigma_1 = \sigma_T \qquad if \;\; 3\sigma_1 + \sigma_3 \geq 0 \quad (6)$$

$$(\sigma_1 - \sigma_3)^2 + 8\sigma_T(\sigma_1 + \sigma_3) = 0 \quad if \;\; 3\sigma_1 + \sigma_3 < 0 \quad (7)$$

where σ_1 the major principal stress (tension), σ_3 the minor principal stress, and σ_T the uniaxial tensile strength of the material.

Thus in the center of the specimen of the Brazilian test (x = y = 0) we obtain

the tensile stress : $\sigma_x = \frac{F}{\pi hR}$ (8)

the compression stress $\sigma_y = \frac{-3F}{\pi hR}$ (9)

Assuming the Hertz solution, the only point where the shear stress is zero, and $3\sigma_1 + \sigma_3 \geq 0$ is the center of the

International Journal of Engineering Research & Technology (IJERT)
ISSN: 2278-0181
Vol. 5 Issue 01, January-2016

specimen. Therefore, the state of stress at this point is exclusively the compression and tension. Thus, if the failure is initiated at the center of the specimen (first cracking), σ_1 correspond to the value of the uniaxial tensile strength. The in-center crack initiation, attributed to tensile failure, represents then a third basic condition to interpret the Brazilian test as an indirect tensile test.

The approach of the analysis of this test is then based on

1-Experimental study of the behavior of the silty soil in different conditions of the split tensile test.

2-Numerical verification of Hertz solution and investigation of the failure mode during the split tensile test.

II. EXPERIMENTAL STUDY

A. Soil characteristics[8]

Tthe experimental work has been conducted in collaboration with the civil engineering department of the National Engineering School of Tunis. Experimental tests were carried out on a silty soil coming from a site that is selected for a landfill project. The physical and mechanical characteristics of the soil are given in Table 1.

Physical and Mechanical Characteristics	
% of size grains < 2 µm	5 %
% of size grain comprising between 2 µm until 80 µm	67 %
Specific density γ_s	26.28 kN/m^3
Void ratio e	0.47
Maximum Dry density (Proctor optimum) γ_{dmax}	17.9 kN/m^3
Optimum water content ω	14.5 %
Plasticity Index PI	13 %
Undrained friction angle ϕ_u	17°
Undrained cohesion C_u	68 kPa

Table 1 Physical and mechanical characteristics of the tested silty soil [8]

B. experimental results

Series of experimental quasi-static tests were carried out on unsaturated silty soil. Initial water content and dry density were kept the same during the tests. In fact the initial water content is fixed to a standard range from the optimum water content (ω_{opt}) to ω_{opt} +2% (the average of the water content is 15.5 % ±1 %, the degree of saturation is 95%). The dry density is almost 95% of the Proctor optimum value and the average of the dry density is 16.5 ±0.5 kN/m^3.

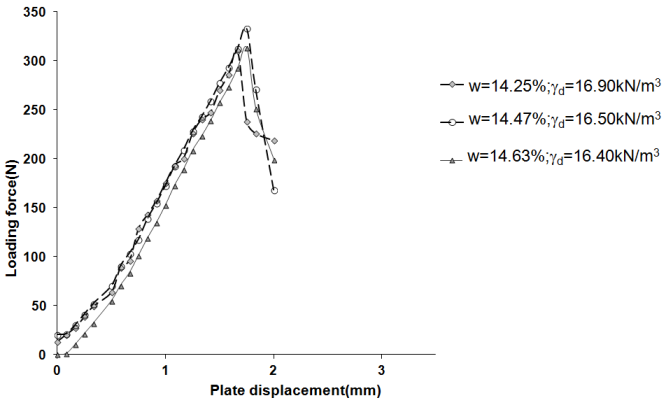

Fig. 1. Loading force versus plate displacement during the split tensile test

The recorded behavior during the tests seems brittle (Figure 1). But the observed failure does not fit the assumed one (Figure 2). Indeed we note an initiation of cracks in the vicinity of loading platens. These cracks propagate toward the center to produce a brittle failure.

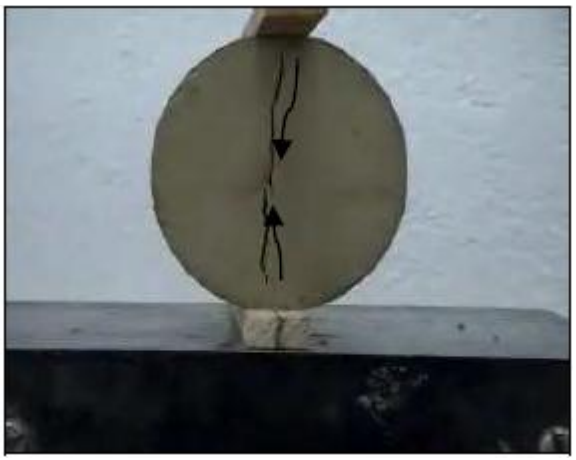

Fig. 2. Failure of the split tensile cylinder

As the first cracks are mainly due to the concentration of the shear stresses in the vicinity of the loading platens, we have created two diametrically opposite flattened portions to facilitate tensile failure (figure 3).

The flattening was defined by the central angle described in Figure 3.

International Journal of Engineering Research & Technology (IJERT)
ISSN: 2278-0181
Vol. 5 Issue 01, January-2016

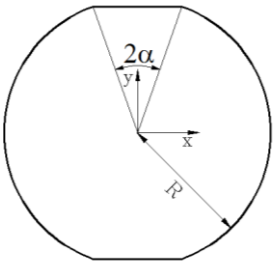

Fig. 3. Flattened cylinder of the split tensile test

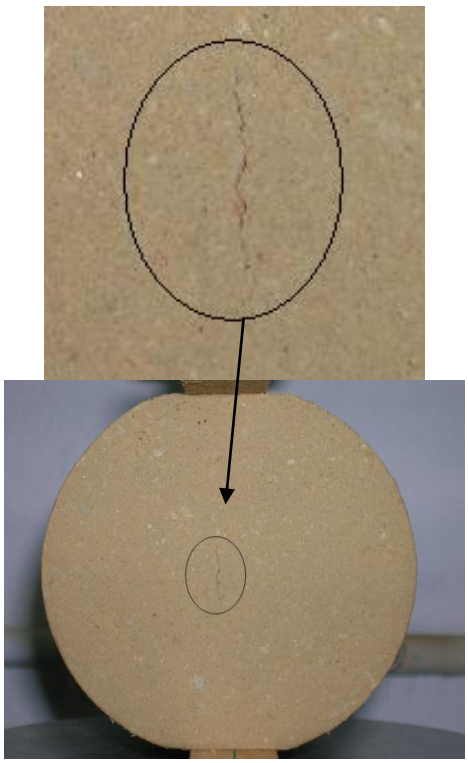

Fig. 4. In-center crack initiation in the flattened cylinder

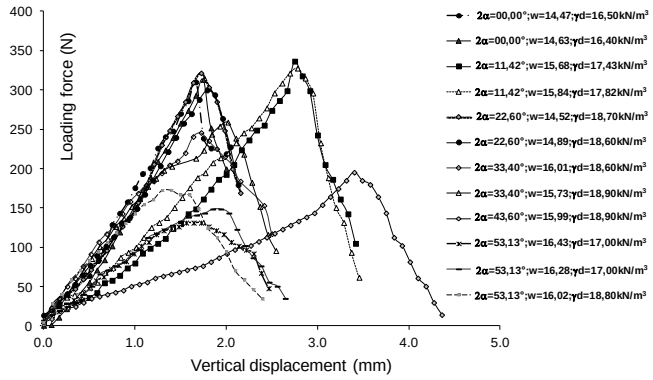

Fig. 5. Loading force versus vertical displacement at different flattening

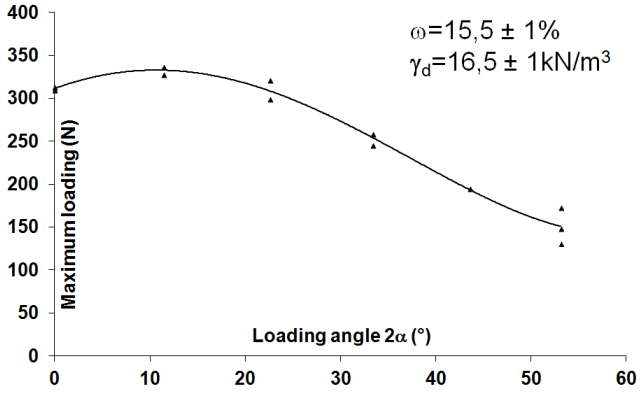

Fig. 6. Variation of the failure loading with the flattening angle

For an angle 2α between 10° degrees and 20° degrees, it was observed that the failure is initiated by a crack in the center (figure 4).

The curves of figures 5 and 6 show the behavior during the splitting test at different flattening.

A numerical investigation was conducted via a discrete elements model. After the calibration of the model based on the experimental results, the Hertz solution was verified, the failure mode and the in-center crack initiation conditions.

III. NUMERCIAL STUDY

A. Numerical model [8]

In order to investigate the crack initiation and the failure mode, a discrete element model (DEM) was developed to simulate the split tensile test (figure 7). In fact, simulation was conducted with Particle Flow Code (PFC2D).

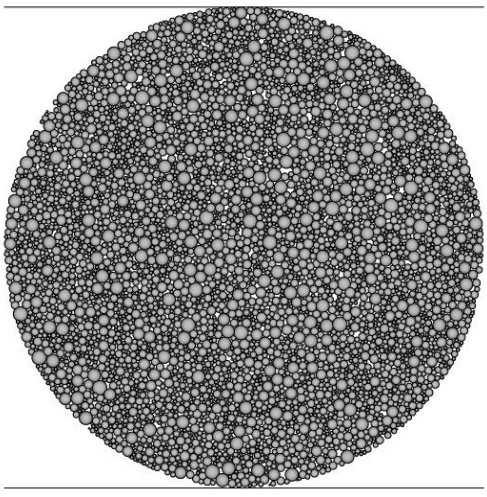

Fig. 7. Modeling of the Brazilian test with DEM

In this study, the contact laws are described by five rheological parameters: normal and tangential stiffness (K^n and K^s), maximum normal and shear strengths (C^n and C^s) and friction coefficient (μ). It is assumed that the parameters of two particles in contact act in series (Figure 8).

International Journal of Engineering Research & Technology (IJERT)
ISSN: 2278-0181
Vol. 5 Issue 01, January-2016

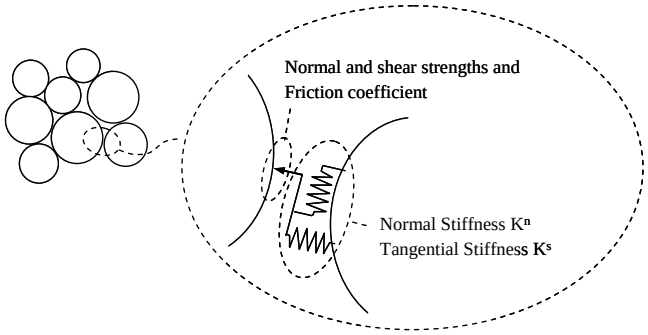

Fig. 8. The rheological model of the DEM

The stiffness model, in correlation with the elastic behaviour material, is a function of the normal and tangential stiffness. The normal and tangential components of the contact forces (F^n and F^s) are proportional, respectively, to the overlap between two discs in contact and to the tangential displacement at contact.

The corresponding basic equations used to define the contact laws between two particles are:

$$F_i^n(t) = K^n U_i^n(t) \quad (10)$$

$$\Delta F_i^s = -K^s \Delta U_i^s \quad (11)$$

$$F_i^s(t) = F_i^s(t - \Delta t) + \Delta F_i^s \quad (12)$$

Where F_i^n and F_i^s are respectively the normal and tangential forces at contact (i) between two particles. Also, U_i^n and ΔU_i^s are respectively the normal and relative tangential displacements at contact (i). (Δt) is a time step during the particle movement. The stiffness contact parameters are computed in PFC2D as:

$$K^n = \frac{K^{ni} K^{nj}}{K^{ni} + K^{ni}} \quad (13)$$

$$K^s = \frac{K^{si} K^{sj}}{K^{si} + K^{sj}} \quad (14)$$

Where K^{ni}, K^{nj} are the normal stiffness moduli and K^{si}, K^{sj} are the tangential stiffness moduli of the particles i and j. The failure behavior is defined by a Coulomb–like slip model. The adhesion at contact of two particles is defined by normal and tangential local adhesions C^n_f and C^s_f. The adhesions serve to limit the total normal and shear forces that the contact can carry by enforcing adhesion-strength limits. Hence, the tensile and shear strengths, C^n and C^s, of a contact between two particles of diameters d_i and d_j are computed in PFC2D as:

$$C^n = C_f^n \min(d_i, d_j) \quad (15)$$

$$C^s = C_f^s \min(d_i, d_j) \quad (16)$$

The tangential component of the contact force is limited in magnitude with a Coulomb-like slip model, with friction coefficient μ. At each step of computation the reliable contacts are re-actualized according to conditions:

$$|F^s| \geq F^s_{\max} \quad (17)$$

$$F^n \geq C^n \quad (18)$$

$$F^s_{\max} = \max\left(\mu |F^n|, C^s\right) \quad (19)$$

B. *Numerical micro parameters [8]*

Quantitative results obtained with an initial set of parameters show that the failure mechanism of the silty soil is well reproduced by the numerical model (behaviour law, cracking zone and failure mode). Figures 9 and 10 show that the failure mechanisms and the response of the material in experimental and numerical tests are identical.

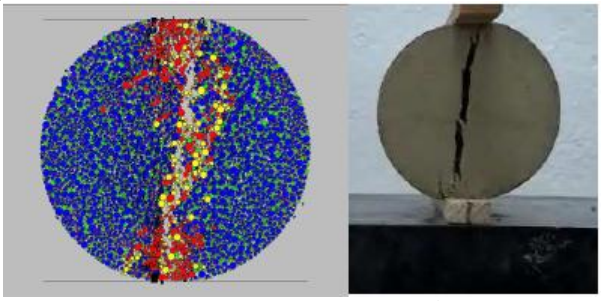

Fig. 9. Numerical and experimental failure

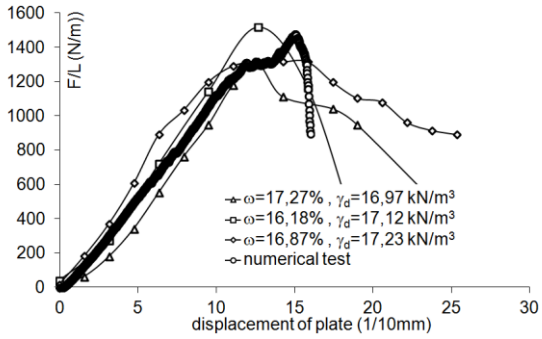

Fig. 10. Numerical and experimental tests results

The fitting of the micro parameters was done in order to reproduce the whole experimental results. Once the split tensile test is well reproduced, the micro-parameters retained to fit the experimental results are those given in table 2.

Micro-parameters		
K^n	14	MN/m
K^s	14	MN/m
C_f^n	150	kN/m
C_f^s	150	kN/m
μ	0.4	
Porosity	0.17	
Density of particles	18	Particles/cm²

Table 2 Micro-parameters used in the numerical model

C. *Stresse distribution in the specimen during the split tensile test*

In the sample the stresses are calculated in measurement circles uniformly distributed over the horizontal and vertical axes as shown in Figure 11. The average number of particles

International Journal of Engineering Research & Technology (IJERT)
ISSN: 2278-0181
Vol. 5 Issue 01, January-2016

per measurement circle is 80. Stresses σ_{xx} and σ_{yy} were measured during the test in the center of the circles. Figures 12, 13 and 14 show the evolution, during the test, of the tensile and compressive stresses along the horizontal and the vertical axes.

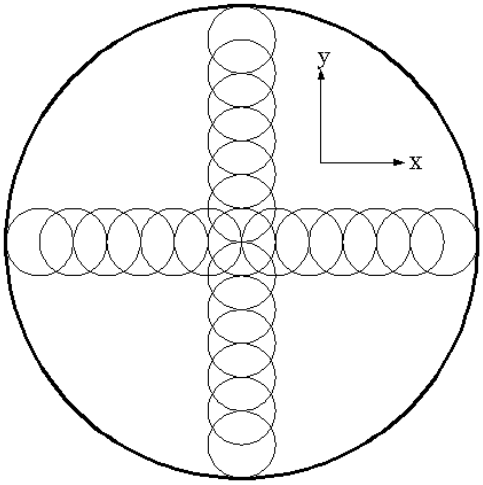

Fig. 11. Positions of the measurement circles in the numerical sample

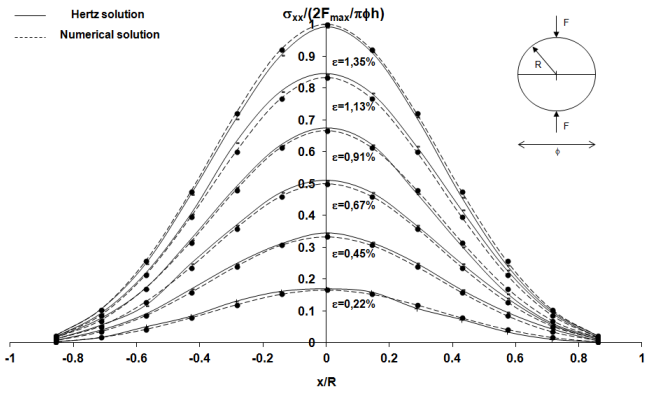

Fig. 12. Comparison between the tensile analytical and numerical stresses along the horizontal axe during the test

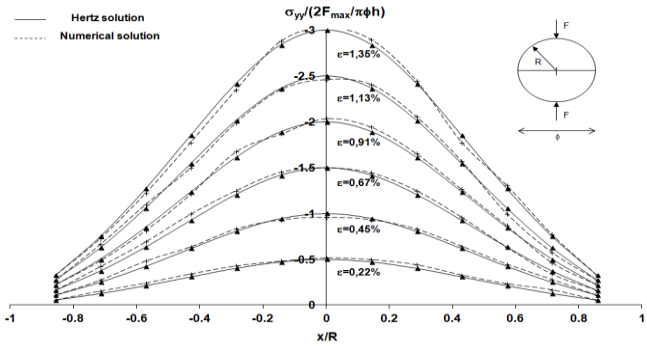

Fig. 13. Comparison between the compressive analytical and numerical stresses along the horizontal axe during the test

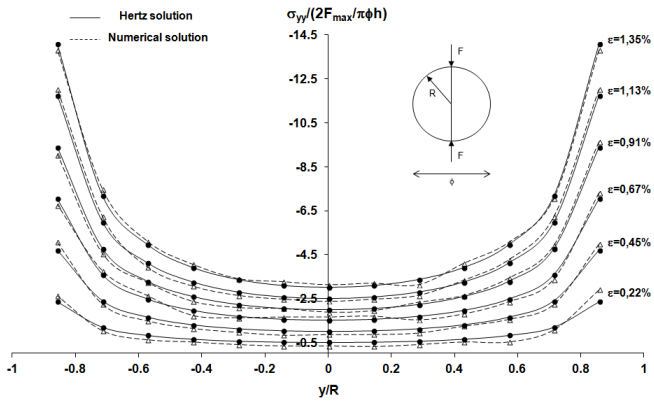

Fig. 14. Comparison between the copressive analytical and numerical stresses along the vertical axe during the test

The stress diagrams presented in Figures 12, 13 and 14 highlight the elastic behavior and thus the suitability of Hertz stress solution. Indeed, an error of less than 3% was recorded between the value of the strain measured in the sample and that calculated by the equations of Hertz.

Figure 15 shows the evolution of compressive and tensile stresses at the center of the specimen during the test. Perfect overlap between the numerical values and the analytical values of the Hertz solution was recorded until failure when a discrepancy occurs. It, therefore, results that the material is linear elastic and obeys the Hertz solution until initiation of failure (ε_{yy} <1.3%).

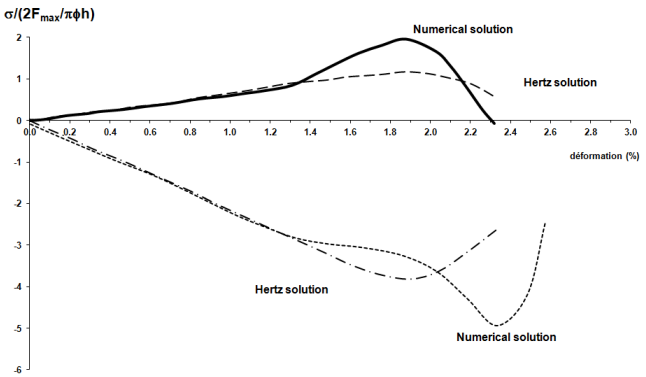

Fig. 15. Analytical and numerical stress - strain curves at the center of the specimen

D. Propagation of cracks and failure of the sample

The location and the nature of the first cracks constitute the basis of the judgment criterion of the validity of the Brazilian test for determining the uniaxial tensile strength. Indeed, the failure must initiate at the center of the sample and shall result only from tensile loads. Figure 16 shows the propagation of microcracks in the sample during the Brazilian test. The microcracks are classified into two categories: normal cracks due to tensile forces and tangential cracks due to shear forces.

International Journal of Engineering Research & Technology (IJERT)
ISSN: 2278-0181
Vol. 5 Issue 01, January-2016

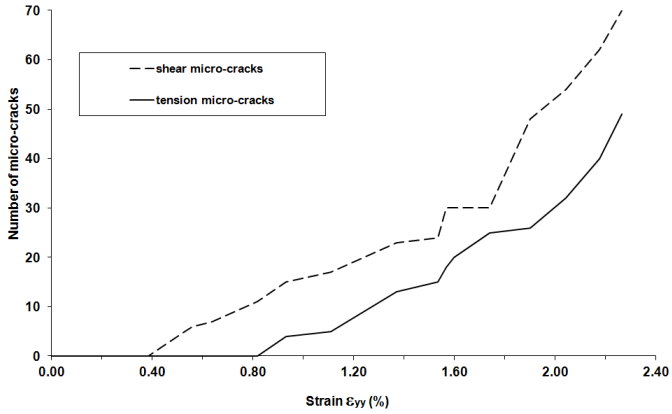

Fig. 16. Evolution of cracks during the split tensile test

Figure 16 shows the appearance at an advanced stage of shear cracks (ε_{yy} = 0.4%). These cracks arise at the upper and lower loading plates (Figure 9). Then after, tensile cracks occur in the central area of the sample, but not necessarily in the center.

In order to study the mode of crack propagation in the sample during the Brazilian test several tests were conducted on samples of different diameters. the maximum tensile stress at the center of the sample was then measured for each diameter (Table 3). In fact, the propagation of cracks in the sample can lead to, either surface failure (Figure 17) or volume failure (Figure 18) or corresponds to an intermediate case between the surface and the volume (essentially surface with microcracks which propagate in the volume surrounding the fracture surface).

D (m)	σ_f(kPa)
0,09	17,05
0,12	15,6
0,15	13,2
0,18	11,7
0,24	10,9
0,3	10,5

Table 3 Maximum tensile stress measured at the center of the specimen versus the diameter

By adopting the assumption that for the quasi - brittle materials, the specific elastic fracture energy is proportional to the square of the split tensile strength [13], we can write:

$$E_r = \lambda\, \sigma_f^2 \qquad (20)$$

Carpinteri and Ferro [14] assume that the specific elastic fracture energy is proportional to the specimen diameter with a certain power.

$$E_r = \beta D^{n-3} \qquad (21)$$

It is noted that for n = 2 the limiting case is obtained which corresponds to the hypothesis of failure of Griffith's theory. It assumes that all of the elastic strain energy is converted or transformed into energy of fracture surface (Figure 18). For n = 3, one obtains the extreme case which assumes that the elastic strain energy is converted into a continuous chain of microcracks distributed throughout the volume of the specimen (Figure 19).

To examine the validity of these assumptions, we write the equality between the two previous expressions of the elastic strain energy, we get:

$$E_r = \lambda\, \sigma_f^2 = \beta D^{n-3} \qquad (22)$$

$$2\log(\sigma_f) = \log(\beta/\lambda) + (n-3)\log(D) \qquad (23)$$

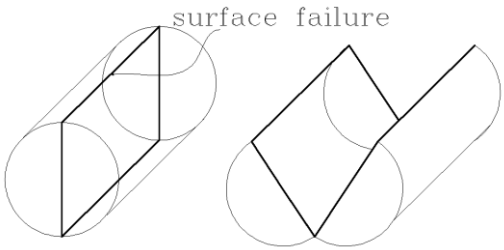

Fig. 17. Surface failure mode

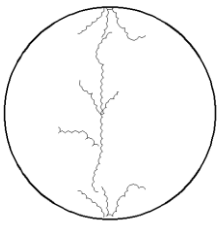

Fig. 18. Volume cracks propagation mode

In other words if the experimental results of Table 1 are reproduced in a logarithmic scale graph, a linear curve fitting gives the following equation:

$$\log(\sigma_f) = A + q\log(D) \qquad (24)$$

The exponent n is written:

$$n = 2q + 3$$

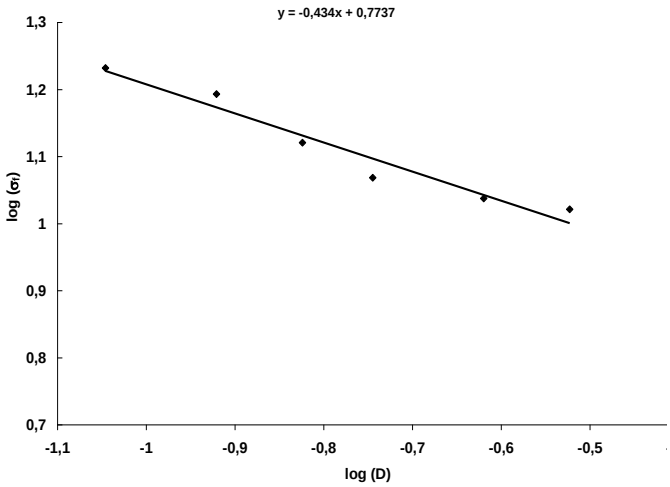

Fig. 19. Split tensile versus the diameter of the test sample

International Journal of Engineering Research & Technology (IJERT)
ISSN: 2278-0181
Vol. 5 Issue 01, January-2016

According to Figure 19, the numerical results of the split tensile test on the silty soil lead to the value n = 2,132.

Thus with n = 2.132, Numerical results is more in agreement with Carpinteri theory, which assumes that all the energy stored in elastic deformation is distributed on an intermediate dimension between a surface and a volume. This result is confirmed by the crack propagation mode observed in figure 9.

As the observed initial crack is not located perfectly in the center of the specimen, one can say that, according to Griffith failure criterion, the maximum tensile stress measured at the center of the sample does not correspond the uniaxial tensile strength. Moreover, by analyzing the stress state at the measurement circles at the vicinity of the load platens, one concludes that these cracks are produced exclusively by an excess of shear stress. Therefore, one could avoid stress concentration by expanding the loading area. Which is to apply the load across a wider surface (through two diametrically opposed flat and whose effort is evenly distributed). The width of the flattening is defined by the angle at the center 2α (Figure 3). Thus, in order to define the optimal flattening which leads to an initial crack in the center, several numerical tests with different flattening were tested. The location of cracks was recorded.

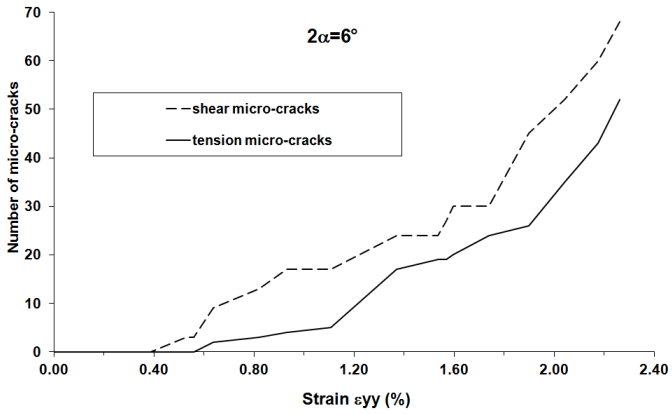

Fig. 20. a. Crack propagation for 2α = 6 °

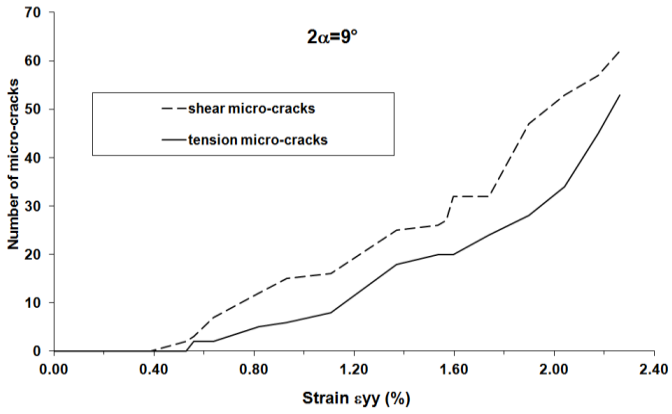

Fig. 20.b. Crack propagation for 2α = 9 °

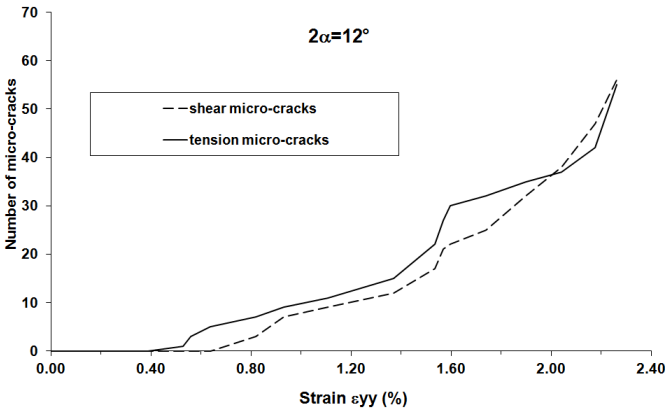

Fig. 20.c. Crack propagation for 2α = 12 °

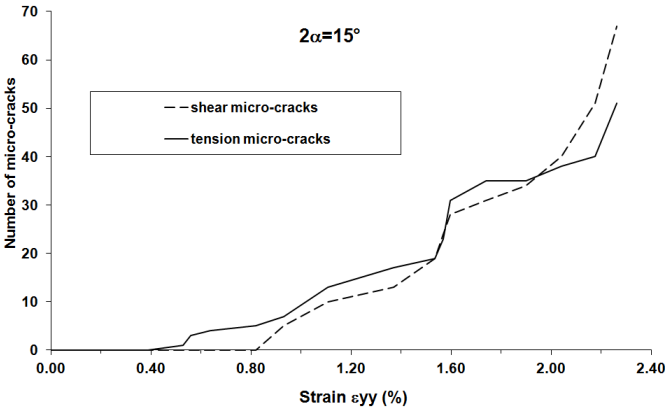

Fig. 20.d. Crack propagation for 2α = 15°

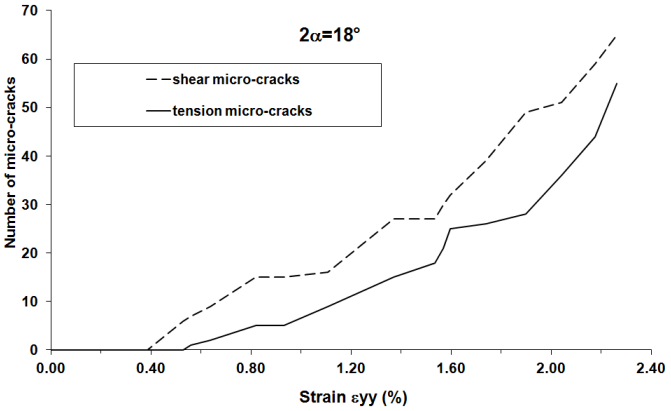

Fig. 20.e. Crack propagation for 2α = 18 °

Figures 20.a to 20.e show the propagation of cracks for flattening angles between 6 ° and 18 °. For $2a$ less than 12 ° the first cracks are caused by shear at the vicinity of the loading platens. Moreover, for $2a$ greater than 15 ° a shear band mode failure was observed. However, for $2a$ between 12 ° and 15 ° a first tensile cracking was observed in the center of the specimen, this fact has been experimentally observed (Figure 6). Thus, a flattening at both loading generators with a central angle between 12 ° and 15 ° can provide a limit tensile stress of the material. In contrast, the value of the tensile stress at the center is not necessarily the uniaxial tensile strength. Indeed, Hertz solution is no longer valid for the new geometry of the flattened cylinder. Consequently, it is proceeded with a numerical check of the main condition: $3\sigma_1 + \sigma_3 \geq 0$.

International Journal of Engineering Research & Technology (IJERT)
ISSN: 2278-0181
Vol. 5 Issue 01, January-2016

Note that this condition is essential to interpret the maximum value of the tensile stress derived from the split tensile test as the uniaxial tensile strength.

It is shown in Figure 21 the variation of $3\sigma_1 + \sigma_3$ at the center of a flat specimen with an angle of 12 °. A negative value was obtained for the strain 1.9% yield point corresponding to the crack initiation at the center of the specimen. Therefore, the split tensile strength does not correspond to the uniaxial tensile strength. However, it remains below the latter.

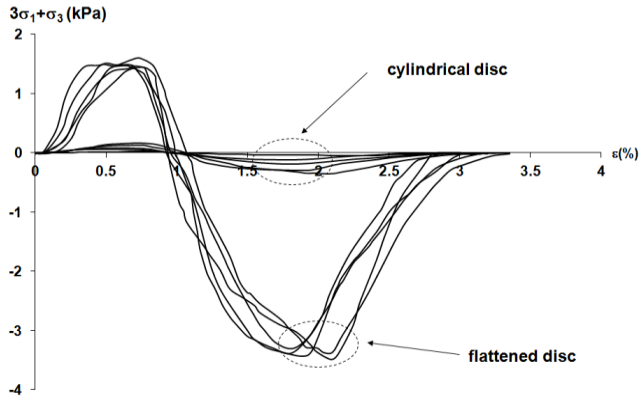

Fig. 21. Variation of $3\sigma_1 + \sigma_3$ in the center of the specimen during the test

E. Conclusion

although the split tensile is the most used for determining the uniaxial tensile strength of rocks and concrete, it should be extended with caution to fine soils. Indeed it has been shown in this work that assumptions of elasticity and brittleness are valid for the silty soil subject of study. However the in-center crack initiation was guaranteed only by a little flattening corresponding to a range between 12° and 15°. For the flattened cylinder , it is shown that the stress distribution no longer corresponds to that proposed by Hertz. Therefore, the use of Griffith failure criterion based on Hertz distribution for this silty soil gives the split tensile strength which is different from the uniaxial tensile strength.

REFERENCES

[1] Somsak S., Hai-Rong L., Tiong-Huan W., "Direct tension test and tensile strain capacity of concrete at early age". Cement and Concrete Research. Volume 33, Issue 12, December 2003, pp. 2077–2084

[2] Mesbah, A., Morel, J., Walker, P., and Ghavami, K. (2004). "Development of a Direct Tensile Test for Compacted Earth Blocks Reinforced with Natural Fibers." J. Mater. Civ. Eng., 10.1061/(ASCE)0899-1561(2004)16:1(95), 95-98.

[3] Heibrock G., Zeh R. M., Witt K. J., "Tensile strength of compacted clays", *Proc. of Int. Conf. "From experimental evidence towards numerical modelling of unsaturated soils*, Germany 18-19 September 2003, Vol. 1, pp. 395-412.

[4] Wang Q. Z., Jia X. M., Kou S. Q., Zhang Z. X., Lindqvist P., 2004, "The flattened Brazilian disc specimen used for testing elastic modulus, tensile strength and fracture toughness of brittle rocks: analytical and numerical results", International Journal of Rock Mechanics and Mining Sciences, Vol. 41, N° 2, pp. 245-253.

[5] Kim, T., Kim, T., Kang, G., and Ge, L. (2012). "Factors Influencing Crack-Induced Tensile Strength of Compacted Soil." J. Mater. Civ. Eng., 10.1061/(ASCE)MT.1943-5533.0000380, 315-320.

[6] Yong Y., Jianmin Y., Zouwu Z., 2006, "Shape effects in the Brazilian tensile strength test and a 3D FEM correction", International Journal of Rock Mechanics & Mining Sciences, Vol. 43, pp. 623–627.

[7] H. Arslan, S. Sture, S. Batiste, 2007, "Experimental Simulation of Tensile Behavior of Lunar Soil Simulant JSC-1", Materials Science & Engineering Vol. A , doi:10.1016/j.msea.2007.05.113.

[8] Ammeri A., Jamei M., Bouassida M., Plé O., Villard P., Gourc J.P, "Numerical study of bending test on compacted clay by DEM: tensile strength determination". *International Journal of Computer Applications in Technology*, Vol. 34, N° 1, 2009, pp. 13-22.

[9] ASTM D3967 - 08 ,Standard Test Method for Splitting Tensile Strength of Intact Rock Core Specimens

[10] ASTM C496 / C496M - 11 , Standard Test Method for Splitting Tensile Strength of Cylindrical Concrete Specimens

[11] Maher, M. and Ho, Y. (1994). "Mechanical Properties of Kaolinite/Fiber Soil Composite." J. Geotech. Engrg., 10.1061/(ASCE)0733-9410(1994)120:8(1381), 1381-1393.

[12] M.R. Mosaddeghi, M.A. Hajabbasi, H. Khademi, "Tensile strength of sand, palygorskite and calcium carbonate mixtures and interpretation with the effective stress theory", Geoderma Volume 134, Issues 1–2, September 2006, Pages 160–170

[13] Kaklis K. N., Vardoulakis I., 2004, "An Experimental Investigation of the Size effect in indirect tensile test on Dionysos marble", *7th National Congress in Theoretical and Applied Mechanics*, Chania 21-26 June.

[14] Carpinteri A., Ferro G., 1994, "Size effects on tensile fracture properties : a unified explanation based on disorder and fractality of concrete microstructure", *Materials and Structures (RILEM)*, Vol. 27, pp. 563-571.